Nonlinear and Intermodulation Characteristics of Millimeter-Wave IMPATT Amplifiers

H. J. KUNO, SENIOR MEMBER, IEEE, AND D. L. ENGLISH, ASSOCIATE MEMBER, IEEE

Abstract—**An analysis and experimental results of intermodulation distortion characteristics of millimeter-wave IMPATT amplifiers are presented. Design considerations for linear IMPATT amplifiers and tradeoffs between the small-signal gain and intermodulation distortion are discussed.**

Introduction

IMPATT-DEVICE technology has rapidly advanced to the point where practical millimeter-wave power sources are now readily available [1]–[6]. In particular, applications of millimeter-wave IMPATT amplifiers in communication systems have recently become important. In many such systems linear power amplification is required. In this paper, nonlinear characteristics and intermodulation distortion of millimeter-wave IMPATT amplifiers are investigated. An analysis and experimental results are presented in detail. Design considerations and tradeoffs for linear millimeter-wave IMPATT amplifiers are discussed.

Nonlinear Characteristics of IMPATT Amplifiers

It has been shown [1] that nonlinear characteristics of a millimeter-wave IMPATT amplifier may be represented by a relatively simplified model such as the one in Fig. 1. In this model the nonlinear negative conductance and avalanche inductance are represented by

$$-G_n = -g_n + \gamma V_d^2$$

$$\frac{1}{L_a} = \frac{1}{l_a} + \lambda V_d^2$$

$$V_d = V_i + V_r \tag{1}$$

where V_d, V_i, and V_r are amplitudes of voltages across the diode terminals, incident wave (input), and reflected wave (output), respectively; $-G_n$ is the voltage-dependent nonlinear negative conductance, $-g_n$ is its small-signal value, γ is a constant; L_a is the voltage-dependent avalanche inductance, l_a is its small-signal value, and λ is a constant.

It has been demonstrated [1] that various nonlinear phenomena and transient responses of millimeter-wave IMPATT amplifiers and injection-locked oscillators can be analyzed accurately starting with this amplifier model. It was also shown [1] that for a stable amplifier, the midband ($\omega = \omega_0 = \sqrt{(1/L_{ext} + 1/l_a)(1/C_j)}$) steady state ($d/dt = 0$) response can be described by

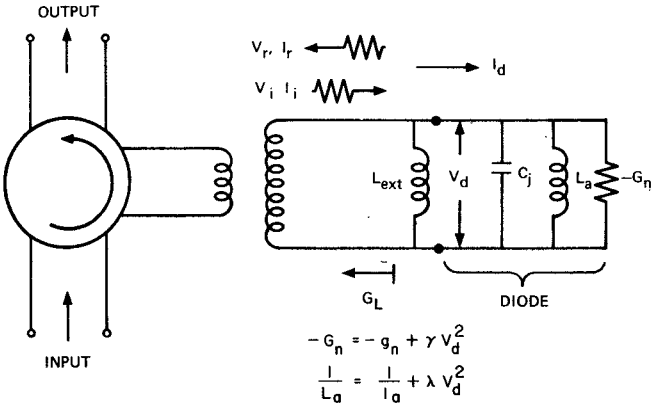

Fig. 1. An equivalent circuit for a circulator-coupled IMPATT amplifier.

$$(A_d^2 - \varepsilon)A_d = \eta A_i$$

$$A_d = A_i + A_r. \tag{2}$$

First consider a case in which the input signal contains a single carrier where A_d, A_r, and A_i are related to V_d, V_r, and V_i as follows:

$$V_d = V_0 A_d \cos(\omega\tau)$$

$$V_r = V_0 A_r \cos(\omega\tau)$$

$$V_i = V_0 A_i \cos(\omega\tau)$$

$$V_0^2 = (4/9)(\omega_0 C_j/\gamma). \tag{3}$$

The output and input powers are related to A_r and A_i in the following manner:

$$P_{out} = (1/2)V_r^2 G_L = (1/2)V_0^2 A_r^2 G_L$$

$$P_{in} = (1/2)V_i^2 G_L = (1/2)V_0^2 A_i^2 G_L. \tag{4}$$

ε and η are determined by the load conductance and the negative conductance of the device:

$$\varepsilon = (g_n - G_L)/(\omega_0 C_j)$$

$$\eta = 2G_L/(\omega_0 C_j). \tag{5}$$

Note that for a stable amplifier

$$G_L > g_n \qquad \varepsilon < 0$$

$$\sqrt{G_0} = \sqrt{\frac{P_{out}}{P_{in}}} = \frac{A_r}{A_i} = \frac{G_L + g_n}{G_L - g_n} \tag{6}$$

where G_0 is the midband small-signal power gain.

Manuscript received March 18, 1976; revised May 10, 1976. This work was supported in part by the Air Force Avionics Laboratory, Air Force Systems Command, U.S. Air Force, Wright-Patterson Air Force Base, OH.

The authors are with Hughes Aircraft Company, Torrance, CA 90509.

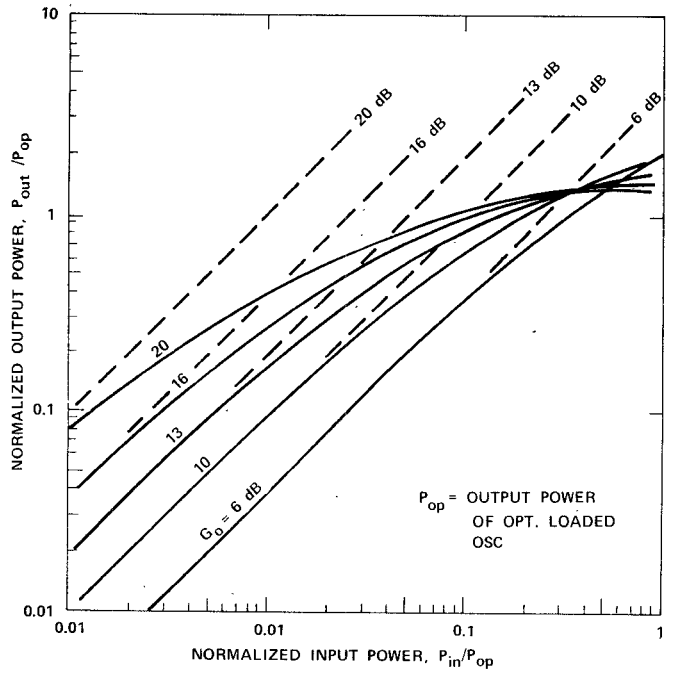

Fig. 2. Normalized output power versus normalized input power of an IMPATT amplifier for several small-signal gain values.

It is convenient to normalize the input and output power levels to the optimally loaded oscillator output power P_{op} [1]:

$$P_{op} = (1/18)(g_n^2/\gamma). \tag{7}$$

For an optimally loaded oscillator,

$$(G_L)_{op} = g_n^2/\gamma$$
$$\varepsilon_{op} = (g_n^2/\omega_0 C_j). \tag{8}$$

For small-signal conditions, i.e., $A_d^2 \ll \varepsilon$, (2) may be reduced to

$$A_d = \left(-\frac{\eta}{\varepsilon}\right) A_i$$

and thus

$$A_r = -\left(\frac{\eta}{\varepsilon} + 1\right) A_i = \sqrt{G_0}\, A_i. \tag{9}$$

Note that

$$-\left(\frac{\eta}{\varepsilon} + 1\right) = \sqrt{G_0}$$

$$\frac{\varepsilon_{op}}{\varepsilon} = -\tfrac{1}{4}(\sqrt{G_0} - 1)$$

$$A_d = (\sqrt{G_0} + 1)A_i$$

$$\frac{A_i^2}{\varepsilon_{op}} = \frac{P_{in}}{P_{op}}. \tag{10}$$

Variations of normalized output power as a function of input for various small-signal gain conditions are calculated from (2) and plotted in Fig. 2 where the output and input are normalized to the optimally loaded oscillator output power.

Shown in Fig. 3(a) are the effects of the signal level and the small-signal gain on the gain compression calculated from (4). Fig. 3(b) shows the measured gain-compression effects of an IMPATT amplifier in the 60-GHz range. Also shown in the figure is the difference in the gain-compression effects between single-tone and two-tone operations. Under the two-tone operation, the gain compression is greater than the single-tone operation. This difference is due to the RF energy diverted from the fundamental to sidebands generated as a result of intermodulation products of the two-tone operation. This will be discussed in the following section. It can be seen that the dynamic range for linear amplification increases as the small-signal gain is reduced. The quality of a linear amplifier is often expressed as the output power at the 1-dB gain-compression point. Effects of the small-signal gain on the dynamic range of linear amplifiers, defined by the 1-dB compression point can be seen in Fig. 3. In order to achieve a large dynamic range for a linear IMPATT amplifier, the amplifier should be tuned for a low small-signal gain.

Intermodulation Distortion

Another measure for the quality of linear IMPATT amplifiers is intermodulation distortion [7]–[9]. When more than one carrier frequency are present in a nonlinear amplifier, multiple sidebands will be generated as intermodulation products. The preceding analysis is now extended to the case where two carriers of equal amplitude are present in the input signal, i.e.,

$$V_i = V_0 A_i(\cos \omega_1 t + \cos \omega_2 t). \tag{11}$$

Equation (2) may be expanded into a series, and for $A_d^2 \ll \varepsilon$

$$A_d = -\left(\frac{\eta}{\varepsilon}\right) A_i \left[1 + \frac{A_d^2}{\varepsilon} + \frac{A_d^4}{\varepsilon^2} + \cdots\right] \tag{12}$$

$$A_r = -\left(\frac{\eta}{\varepsilon} + 1\right) A_i - \left(\frac{\eta}{\varepsilon}\right)(A_i)\frac{A_d^2}{\varepsilon} + \cdots. \tag{13}$$

By substituting (11) and (10) into (12), and separating terms containing the fundamental frequencies ω_1,ω_2 and the first intermodulation products containing $2\omega_1 - \omega_2$, $2\omega_2 - \omega_1$,

$$\omega_1,\omega_2: \frac{P_{out}}{P_{op}} = G_0\left(\frac{P_{in}}{P_{op}}\right) \tag{14}$$

$2\omega_1 - \omega_2, 2\omega_2 - \omega_1$:

$$\frac{I_3}{P_{op}} = \left(\frac{9}{256}\right)(\sqrt{G_0} + 1)^6(\sqrt{G_0} - 1)^2\left(\frac{P_{in}}{P_{op}}\right)^3. \tag{15}$$

The quality of a linear amplifier is often determined by the output power level where the fundamental frequency components of the output and the third-order terms (the first intermodulation products) intercept as shown in Fig. 4. The intercept points are obtained by extending the straight-line portions of the curves. From (14) and (15),

$$\text{IP} = \frac{I_3}{P_{op}} = \frac{P_{out}}{P_{op}} = \left(\frac{16}{3}\right)\frac{(\sqrt{G_0})^3}{(\sqrt{G_0} + 1)^3(\sqrt{G_0} - 1)} \tag{16}$$

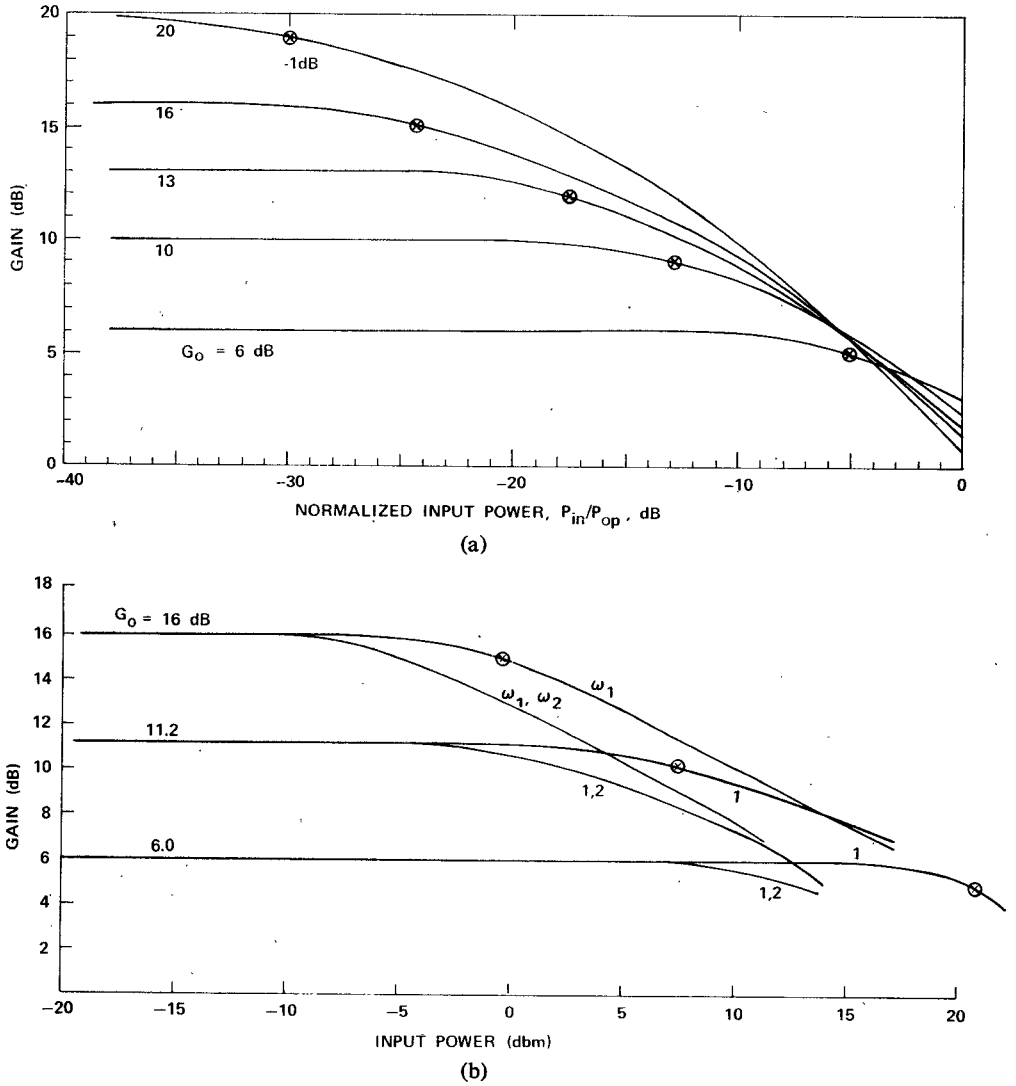

Fig. 3. Gain versus input power of an IMPATT amplifier for several small-signal gain values. (a) Calculated. (b) Measured for single-tone and two-tone inputs.

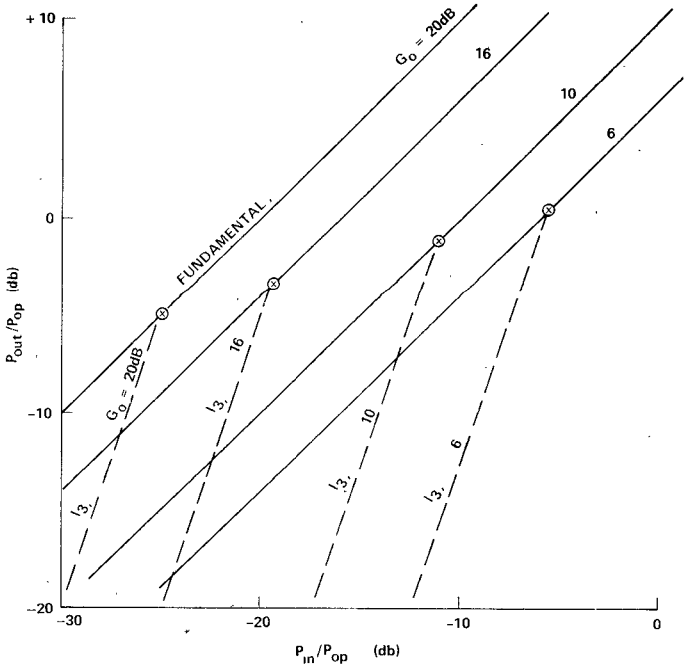

Fig. 4. Normalized third-order intermodulation levels versus normalized input power for several small-signal gain values.

at the intercept point. Note that this value increases as the small-signal gain is decreased. Similarly, by taking the ratio between the intermodulation product and the fundamental,

$$\frac{I_3}{P_{out}} = \left(\frac{9}{256}\right) \frac{(\sqrt{G_0} + 1)^6(\sqrt{G_0} - 1)^2}{G_0} \left(\frac{P_{in}}{P_{op}}\right)^2. \quad (17)$$

These relationships are valid for the small-signal levels where the intermodulation distortion is low enough to be useful for communication systems. (At large-signal levels a larger number of terms must be carried through in (12)–(15).)

Shown in Fig. 5 are the effects of the small-signal gain on the intercept point. It can be seen that, in order to minimize the intermodulation products, the small-signal gain of the amplifier should be made small.

Intermodulation Distortion Characteristics Measurements

The intermodulation distortion characteristics of silicon single-drift high-power IMPATT amplifiers were extensively studied for various bias currents and small-signal tuning conditions. The amplifier circuit configuration and charac-

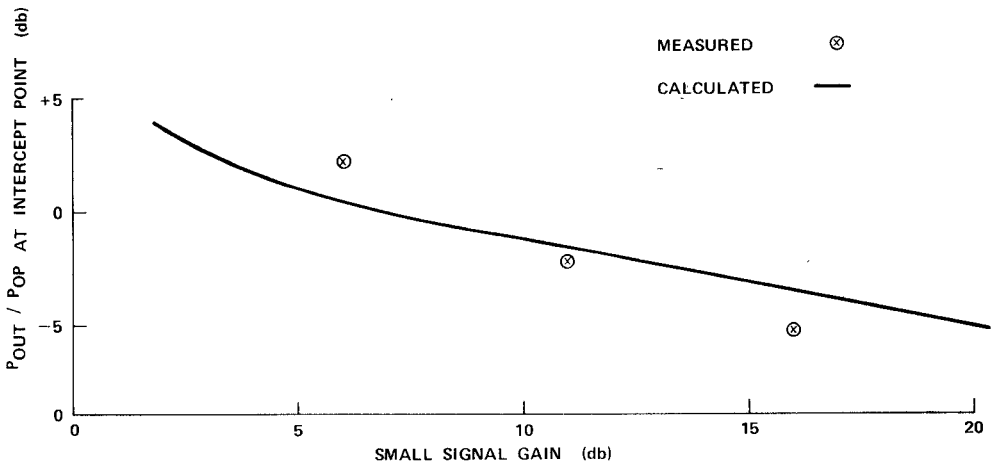

Fig. 5. Normalized intercept point versus small-signal gain.

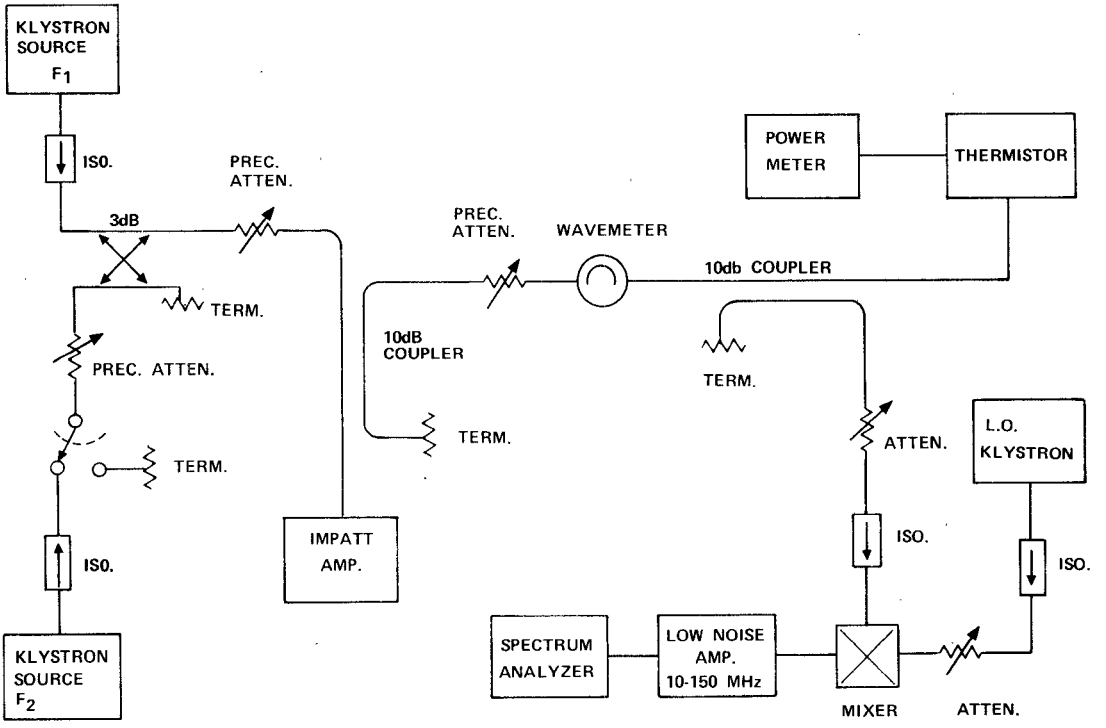

Fig. 6. Experimental test setup for intermodulation distortion measurement.

teristics other than the intermodulation distortion have been reported [1], [2].

A schematic diagram of the test system for measuring intermediate modulation (IM) distortion characteristics with the two-tone signal method is given in Fig. 6. The millimeter-wave mixer was used to convert the IMPATT-amplifier spectrum down to a lower frequency where a commercially available spectrum analyzer could be used. The low-noise video amplifier was used to increase the system sensitivity to low-level IM products and also to filter out higher order mixer conversion products. The IM distortion characteristics of the test system were first checked before the IMPATT amplifiers were measured. With a two-tone input signal, the third-order IM distortion ratio of the system was -55 to -60 dB and much lower for the higher order IM products. For each IMPATT-amplifier measurement, the signal level to the mixer was set to a value where the system IM products were approximately 55 dB below the levels of each of the two-tone input signals so that maximum system sensitivity was obtained. However, when the full amplifier distortion spectrum was presented to the mixer as a "signal," a stacking effect occurred on the higher order products generated in the mixer, making it difficult to determine its contribution to the overall distortion. Therefore, the measured data for the higher order products may be in considerable error, especially for the lower distortion ratios.

Both the intercept point (IP) and the intermodulation distortion ratio were found to be useful in comparing different IMPATT diodes and in evaluating the effects of bias-current and circuit-tuning conditions on amplifier performance. There are two ways of defining the intercept point which differ by 3 dB, but they are consistent in that they both predict the correct IM distortion ratio at lower

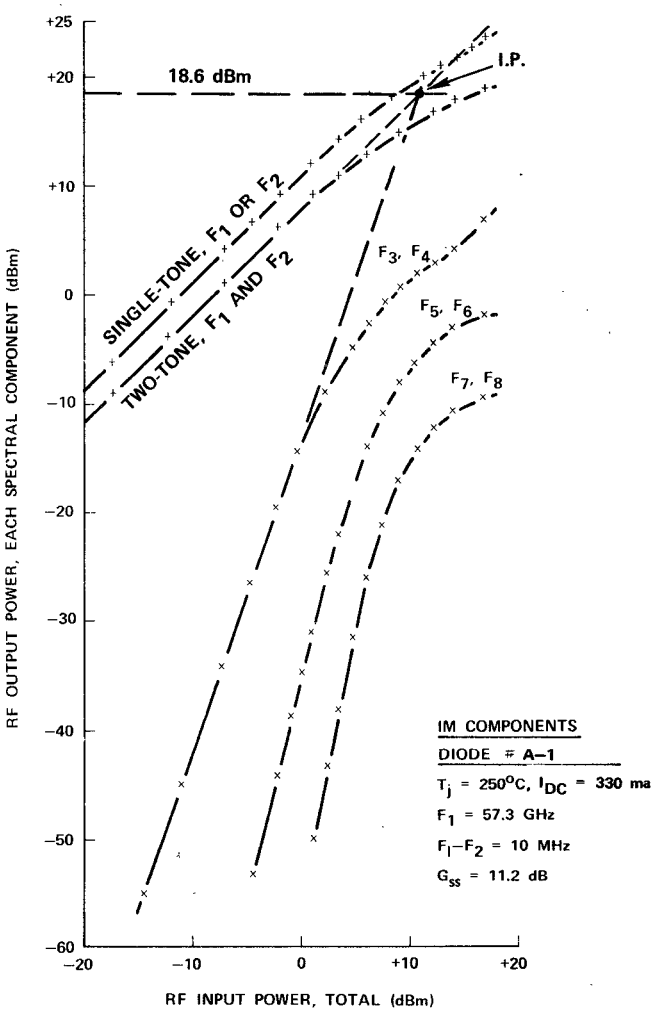

Fig. 7. Single-tone power transfer characteristics and two-tone intermodulation distortion component levels for diode A-1.

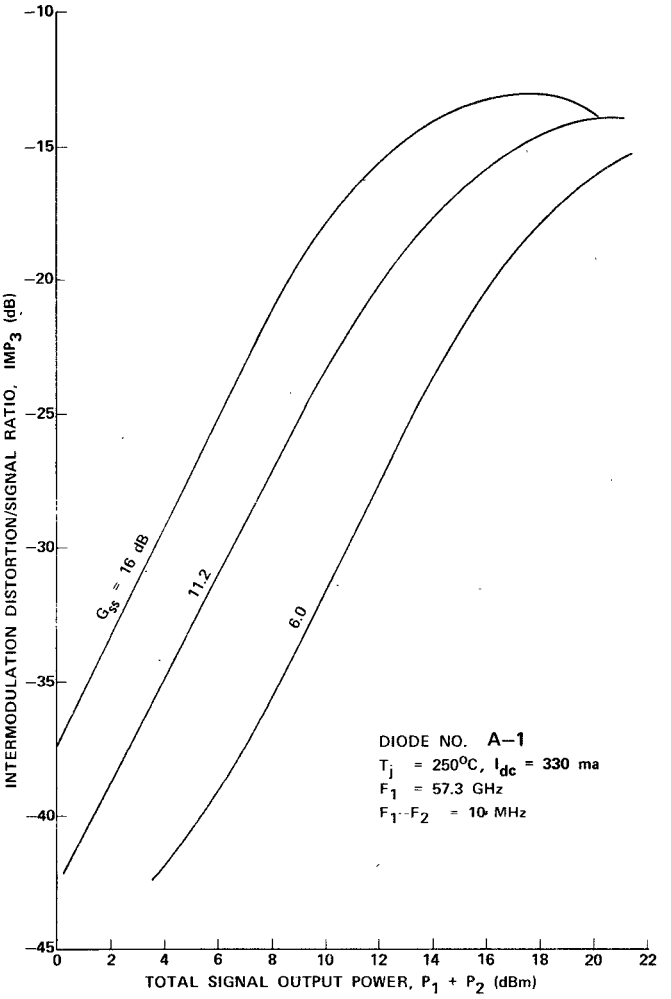

Fig. 8. Intermodulation distortion ratio versus total signal output power for several small-signal gain values and constant bias current.

imput-signal power levels. One method uses the total power in both sidebands of the third-order products and the power of the single-tone fundamental. The other uses the single-sideband powers of the third-order products and the power of the two-tone fundamental. For highest accuracy, all of the intercept points were obtained by taking the mean value of intercepts analytically extrapolated from the data points of the low-level straight-line portions of the curves.

In Figs. 7–12 intermodulation characteristics are presented for two high-power single-diode IMPATT amplifiers. Diode A-1 had a breakdown voltage of 13.5 V and a junction area of approximately 1.8×10^{-5} cm^2. The corresponding parameters for diode B-2 were 15 V and 2×10^{-5} cm^2.

In Figs. 7 and 10, examples of the single-tone and two-tone power transfer curves are given for each of the two diodes, as well as the curves of the first three sets of distortion products. The single-tone and two-tone curves are identical at low power levels, but the separation becomes greater at higher power levels where more of the fundamental power is converted into sideband power. These figures also show how the single-sideband intercept points are determined graphically. Single-sideband intercept values are used exclusively in the following discussion of amplifier performance.

Fig. 8 shows the effect of varying the small-signal gain while maintaining a constant bias current and junction temperature for diode A-1. The small-signal gain was varied by adjusting the circuit-tuning elements. Intercept points of 23.0, 18.6, and 15.5 dBm were obtained for small-signal gain settings of 6, 11, and 16 dB, respectively. It can be seen from this figure that the highest output power with lowest distortion is achieved with the small-signal gain set as low as is practical. For example, if a maximum distortion ratio of 17 dB below the signal power level is arbitrarily chosen, the total two-tone output power must be limited to smaller than 12.5 mW with the 16-dB gain amplifier. However, the 6-dB gain amplifier can be driven up to an 80-mW output before the 17-dB distortion level is reached. These results are in good agreement with the preceding analysis.

Fig. 9 shows the effect of dc-bias-current and junction-temperature variations on intermodulation distortion while maintaining the small-signal gain constant for diode A-1. The gain was kept constant by readjusting the circuit tuning at each bias current. The measured intercept points were 23.0, 21.6, and 19.6 dBm for diode junction temperatures of 250, 208, and 169°C, respectively. The corresponding bias currents are given in the figure. The preceding analysis shows

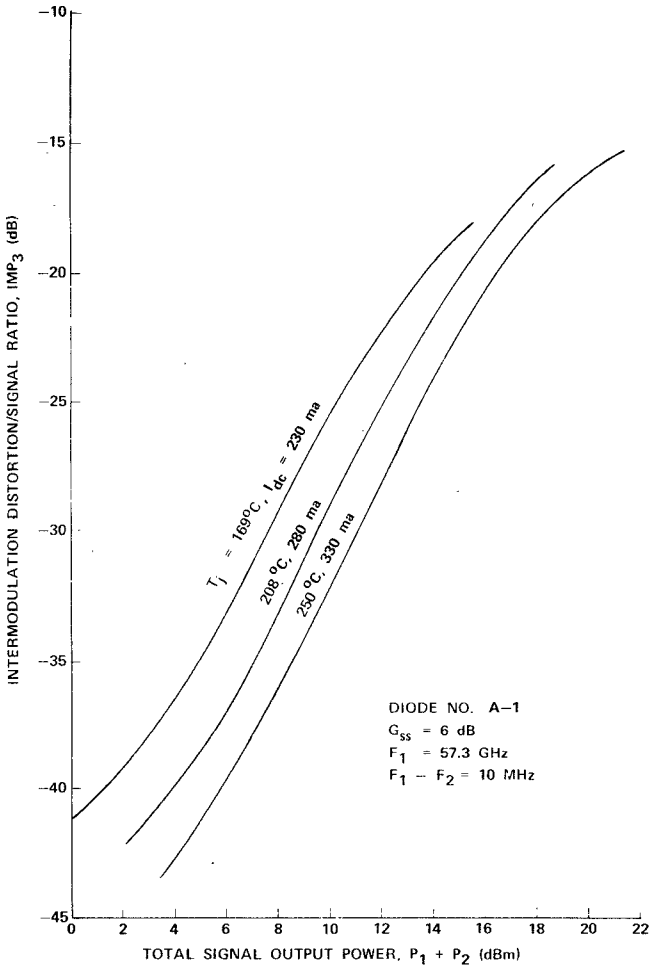

Fig. 9. Intermodulation distortion ratio versus total signal output power for several bias-current values and constant small-signal gain.

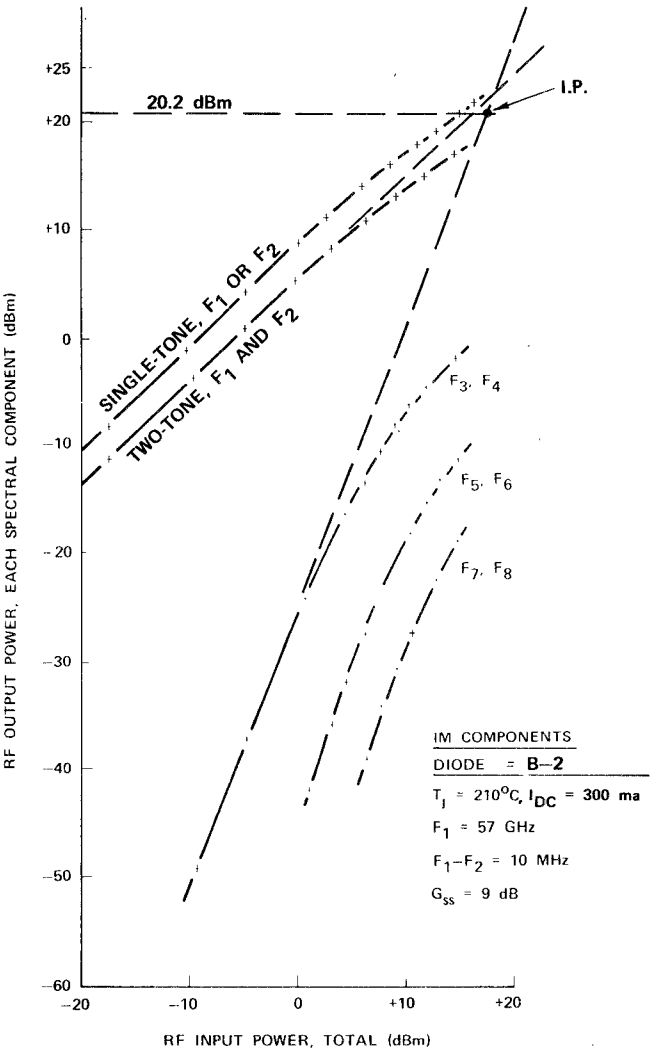

Fig. 10. Single-tone power transfer characteristics and two-tone intermodulation distortion component levels for diode B-2.

that the intercept point is directly proportional to the output power of the optimally loaded oscillator. For the bias-current and junction-temperature range of these tests, oscillator power variations of about 4 dB were observed with this diode.

Fig. 11 shows the IM distortion characteristics for diode B-2 for two different bias currents with a fixed tuning condition where the small-signal gain was not maintained constant, i.e., no circuit retuning was done as the bias current was changed. The gain for the higher temperature was 12.6 dB and 9 dB for the lower temperature. Surprisingly, the IP increased from 18.5 to 20.2 dBm as the junction temperature was reduced from 252 to 210°C, corresponding to bias currents of 360 and 300 mA, respectively. If the 17-dB IM ratio is again chosen as a maximum allowable distortion, the maximum output power is 30 mW for the higher bias current; whereas, for the lower bias current, the IM ratio is still smaller than 17 dB at the highest output level used in the measurement, 100 mW. The power of an optimally loaded oscillator was found to vary by about 2 dB over this bias current range. As predicted by the preceding analysis, the change in small-signal gain dominates over the change in optimum power in determining the distortion ratio.

Fig. 12 shows the two-tone spectrum analyzer traces of amplifier B-2, operating at the higher bias current and returned slightly, for several different total output-signal power levels.

The experimental data presented here demonstrate that IM distortion levels are not as sensitive to diode bias current as to the small-signal gain, provided that the amplifier is operated at RF drive levels below the point where significant gain compression starts to occur. Note, however, that the output power level for the onset of gain compression is dependent on bias current as well as the small-signal gain.

The intermodulation characteristics of a four-diode power amplifier/combiner were also measured. Fig. 13 gives the IM characteristics of the four-diode power amplifier/combiner [10]. Comparing these curves with those for a single diode with comparable gain shows that the IP is 6 dB higher for the combiner (24.5 dB versus 18.6 dB). At the 17-dB distortion-ratio points, the combiner total signal output power is 200 mW compared to 32 mW for the single diode. At lower output power levels, the combiner yields approximately 6 dB more output power for any given IM ratio. Thus combining diodes is an effective means of

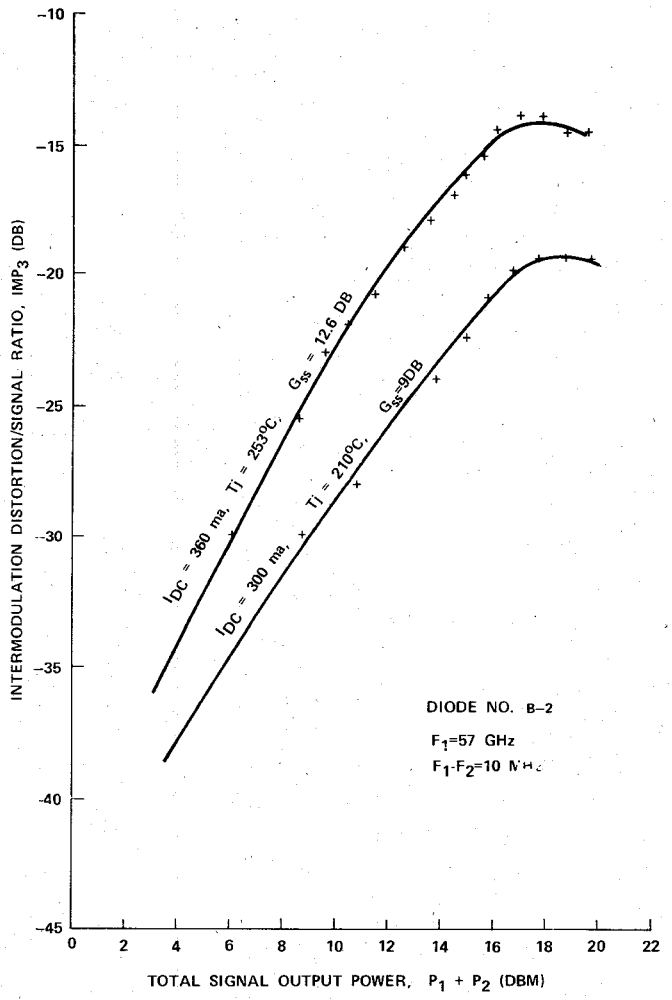

Fig. 11. Intermodulation distortion ratio versus total signal output power, gain allowed to vary with bias current.

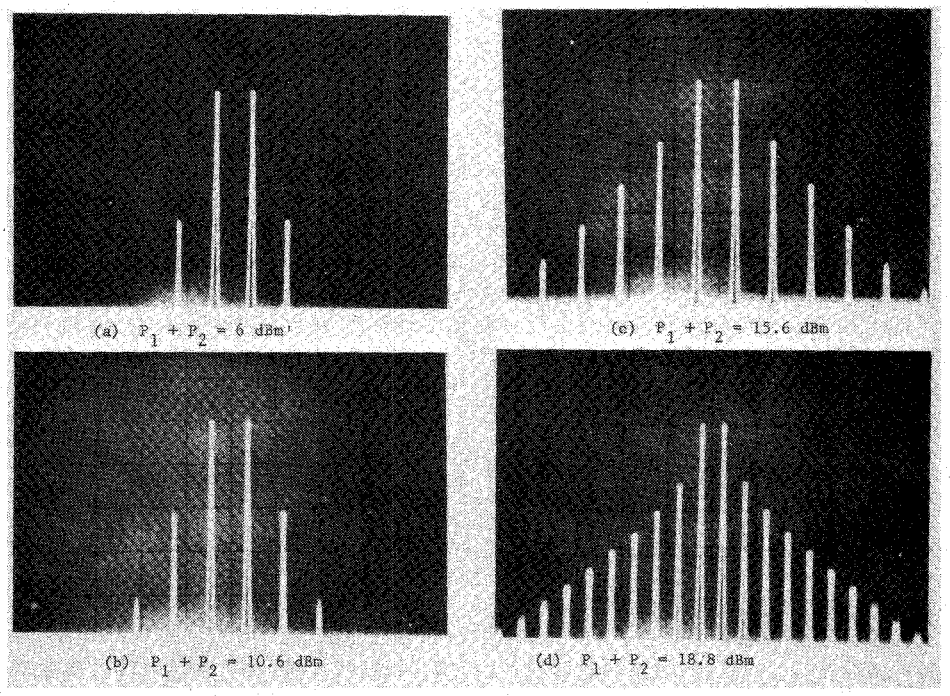

Fig. 12. Intermodulation distortion spectrum of diode B-2.

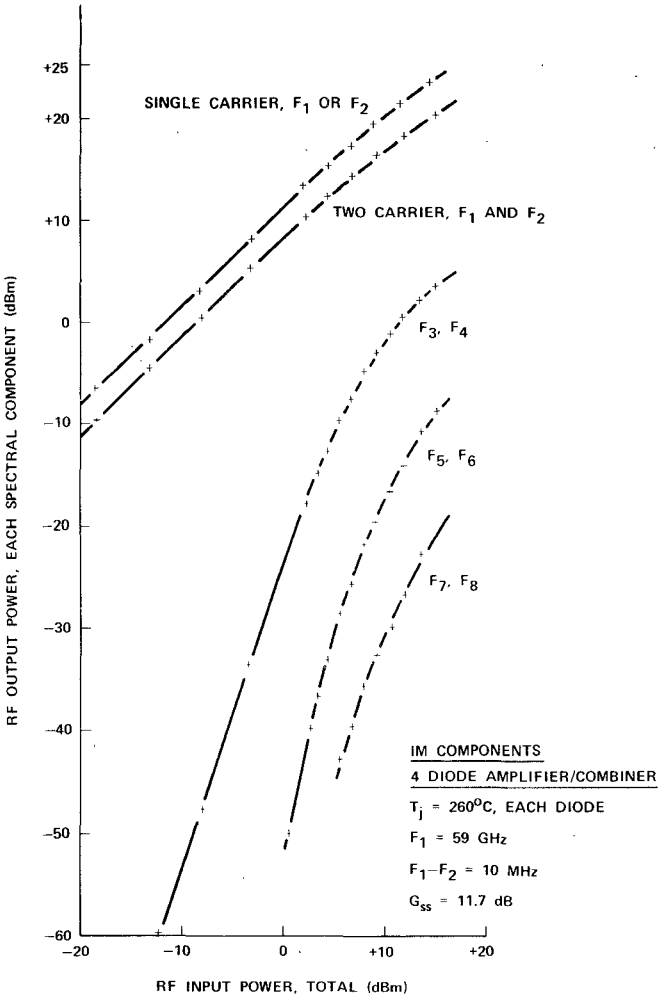

Fig. 13. Single-tone power transfer characteristics and two-tone intermodulation distortion component levels for four-diode power amplifier/combiner.

improving performance to achieve a larger dynamic range of linear amplification, i.e., lower intermodulation distortion. Similar improvement can also be expected with high-power double-drift IMPATT amplifiers.

Conclusion

Intermodulation distortion characteristics of millimeter-wave IMPATT amplifiers have been analyzed and investigated experimentally. It was shown that, in order to achieve a high dynamic range for linear amplification, the small-signal gain should be made low and a diode with high output power capability should be used. Design curves for output power levels at the 1-dB gain-compression point and at the interception point between the fundamental and first intermodulation products, and the gain variation with the input power level have been derived as explicit functions of the small-signal gain and the output power capability of the diode. These curves are useful for estimating the intermodulation products and the dynamic range for IMPATT amplifiers.

References

[1] H. J. Kuno, "Analysis of nonlinear characteristics and transient response of IMPATT amplifiers," *IEEE Trans. Microwave Theory Tech.*, vol. MTT-21, pp. 694–702, Nov. 1973.
[2] H. J. Kuno and D. L. English, "Nonlinear and large-signal characteristics of millimeter-wave IMPATT amplifiers," *IEEE Trans. Microwave Theory Tech.*, vol. MTT-21, pp. 703–706, Nov. 1973.
[3] H. Hayashi *et al.*, "80 GHz IMPATT amplifier," in *1974 ISSCC Digest of Technical Papers*, vol. XVII, pp. 102–103, Feb. 1974.
[4] Y. Chang, H. J. Kuno, and D. L. English, "High data-rate millimeter-wave transmitter module," *IEEE Trans. Microwave Theory Tech.*, vol. MTT-23, pp. 470–477, June 1975.
[5] K. P. Weller, R. S. Ying, and E. M. Nakaji, "Millimeter-wave 94 GHz silicon IMPATT amplifiers," in *1975 ISCC Digest of Technical Papers*, vol. XVIII, pp. 128–139, Feb. 1975.
[6] T. Miyakawa *et al.*, "Wideband tunable and highly stabilized millimeter-wave IMPATT oscillators," in *1975 IEEE-MTT Microwave Symp. Digest of Technical Papers*, pp. 222–223, May 1975.
[7] D. F. Peterson and D. H. Steinbrecher, "Circuit model for characterizing the nearly linear behavior of avalanche-diodes in amplifier circuits," *IEEE Trans. Microwave Theory Tech.*, vol. MTT-21, pp. 19–27, Jan. 1973.
[8] R. J. Trew, N. A. Masnari, and G. F. Haddad, "Intermodulation characteristics of X-band IMPATT amplifiers," *IEEE Trans. Microwave Theory Tech.*, vol. MTT-20, pp. 805–812, Dec. 1972.
[9] E. F. Scherer, "Large-signal operation of avalanche-diode amplifiers," *IEEE Trans. Microwave Theory Tech.*, vol. MTT-18, pp. 922–932, Nov. 1970.
[10] H. J. Kuno and D. L. English, "Millimeter-wave IMPATT power amplifier/combiner," this issue, pp. 758–767.